A simple locally active memristor and its application in HR neurons

Cite as: Chaos **30**, 053118 (2020); https://doi.org/10.1063/1.5143071
Submitted: 20 December 2019 . Accepted: 22 April 2020 . Published Online: 08 May 2020

Yumei Tan, and Chunhua Wang

A simple locally active memristor and its application in HR neurons

Cite as: Chaos **30**, 053118 (2020); doi: 10.1063/1.5143071
Submitted: 20 December 2019 · Accepted: 22 April 2020 ·
Published Online: 8 May 2020

Yumei Tan[a] and Chunhua Wang[b]

AFFILIATIONS

College of Computer Science and Electronic Engineering, Hunan University, Changsha 410082, China

[a]**E-mail:** tan5191214@163.com
[b]**Author to whom correspondence should be addressed:** wch1227164@hnu.edu.cn

ABSTRACT

This paper proposes a simple locally active memristor whose state equation only consists of linear terms and an easily implementable function and design for its circuit emulator. The effectiveness of the circuit emulator is validated using breadboard experiments and numerical simulations. The proposed circuit emulator has a simple structure, which not only reduces costs but also increases its application value. The power-off plot and DC *V-I* Loci verify that the memristor is nonvolatile and locally active, respectively. This locally active memristor exhibits low cost, easy physical implementation, and wide locally active region characteristics. Furthermore, a neural model composed of two 2D HR neurons based on the proposed locally active memristor is established. It is found that complicated firing behaviors occur only within the locally active region. A new phenomenon is also discovered that shows coexisting position symmetry for different attractors. The firing pattern transition is then observed via bifurcation analysis. The results of MATLAB simulations are verified from the hardware circuits.

The memristor is the fourth fundamental circuit element. Due to its nanoscale, nonlinearity, and memorability characteristics, memristors play a significant role in exploring nonlinear dynamic behaviors. Local activity is considered as the origin of complexity. Some locally active memristor emulators have been created to enrich memristor theory and study new nonlinear dynamics. However, in related works, the simulation models of locally active memristors consist of complex functions, which increase the difficulty of circuit implementation. This paper proposes a simple locally active memristor and its circuit emulator, which exhibit a simple structure and excellent characteristics such as low cost, easy physical implementation, and a wide locally active region. In addition, because of their natural biomimetic properties, memristors are usually used to imitate biological synapses and autapses. Thus, a new neural model based on the proposed locally active memristor is established, which shows more complex firing behaviors within the locally active region. A new neurodynamic behavior is discovered for coexisting position symmetry with different attractors.

I. INTRODUCTION

The memristor was originally postulated by Chua[1] and is the fourth basic circuit element defined by a constitutive relationship between charge and magnetic flux. Memristors were then physically implemented and fabricated by Hewlett–Packard Lab in 2008.[2] Since then, numerous researchers and scholars have focused on memristors and their applications. Due to their low power consumption, nanometer size, and nonvolatile characteristics, memristors can be applied in a variety of scenarios, such as neural networks,[3–6] memory storage,[7,8] chaotic circuit design,[9–11] and secure communications.[12]

Local activity as defined by Chua in 2014[13] is considered as the origin of complexity[14,15] as it provides an effective way to study complicated nonlinear dynamic behaviors. Therefore, the research on locally active memristors can be divided into two categories: elements and emulators. In 2017, a locally active memristor element called the nanoscale NbO2 Mott memristor was physically implemented,[16] which showed that it is suitable for analog computing. However, due to the cost and technical difficulties of nanoscale device manufacturing, commercially available locally active memristor elements are infeasible for the near future. Therefore, to enrich theoretical knowledge of locally active memristors and explore their applications in various fields, studies of locally active emulators and their simulation models are necessary. A locally active memristor, which is called the Chua Corsage memristor,[17] was designed by Chua. Its state equation was composed of piecewise linear functions, and its locally active range is limited. Furthermore, Kim *et al.* performed a detailed analysis of the complex frequency domain

and bifurcation characteristics of the Chua Corsage memristor.[18] A bi-stable bi-local active memristor was then proposed by Chang *et al.*[19]

At the same time, the complex frequency domain and bifurcation characteristics of the memristor are analyzed. The memductance function of the bi-stable bi-local active memristor was realized using a square function, which may limit its range. Jin *et al.*[20] introduced a locally active memristor and designed a nonlinear circuit to verify its characteristics. Both the memductance function and state equation were realized using a cubic function, which increased the cost of circuit implementation. Previous studies were limited in exploring the simulation models of locally active memristor emulators. In this paper, a simple locally active memristor emulator and its circuit emulator consisting of linear terms and an easily implemented function are proposed. The memductance of the locally active memristor can be positive, zero, and negative. The locally active memristor emulator not only has a simple structure but also exhibits a wide memductance range, locally active region, low cost, and easy physical implementation characteristics.

It is well-known that memristors are natural candidates to mimic biological synapses[21,22] and autapses.[23,24] Accordingly, the application of memristors, including ordinary and locally active memristors, in neural networks is an important research topic. Previous works have applied numerous ordinary memristors in neurons and neural networks to study brain electrical activities where the memristor relation emphasizes the memory characteristics of neurons. Synapses are important bridges that connect different neurons. Faraday's law of electromagnetic induction states that a floating neuron membrane potential generates an induction current that behaves like a memristor. Thus, some scholars have suggested that neurons should be connected via memristor synapses. They have found that memristor synapses promote the synchronization stability of neurons[25,26] and that the neuron firing behaviors simultaneously change when varying the memristance.[27] An autapse is a connection between a neuron and itself via a closed loop. Some improved neuron models that consider memristors as autapses have been established, which discovered different firing pattern transitions under the influence of autapses.[28–30] The self-connection resistor of artificial neural networks, such as the Hopfield network, is replaced by a memristor autapse. As the memristance state is related to the initial state of the memristor nonvolatility, memristive Hopfield networks tend to induce multi-stable patterns under different initial conditions.[31,32] There is evidence that neurons operating in a locally active region may be central to learning efficiency, adaptability, and analog computing in the brain.[33]

Chua proved that the potassium and sodium ion channels distributed over the entire length of the axons in neurons are locally active memristors.[34,35] Thus, the research on the application of locally active memristors in neural networks is of great importance. However, there have been no further studies on their application in neural networks. As is well-known, the HR neuron is effective and available to mimic electrical activities in the brain.[25–30] This paper establishes a neural model composed of two HR neurons using the proposed locally active memristor as an autapse. It is found that more complicated firing behaviors are generated for all the states in the locally active region based on bifurcation analysis. Of note, compared with neural models constructed from ordinary memristors,[25–32] the proposed neural model induces the coexistence position symmetry of different firing behaviors, which has not been reported in neurons to date.

This paper is organized as follows. A generic memristor model based on Chua theory and its circuit emulator are presented, and the nonvolatile and locally active characteristics are verified using the power-Off plot (POP) and DC V-I Loci, respectively. The bi-stable pinched hysteresis loops of the proposed locally active memristor are simulated in Sec. II, and a neural model based on the locally active region is established in Sec. III. The electrical activities of the neural model are numerically revealed using bifurcation diagrams, Lyapunov exponents, and phase portraits in Sec. IV, while Sec. V provides a circuit implementation of the proposed neural model. Section VI summarizes the work.

II. LOCALLY ACTIVE MEMRISTOR MODEL

Chua[17] defined a generic memristor and presented its mathematical definitions, which are shown as follows:

$$y(t) = G(x)u(t), \tag{1}$$

$$\frac{dx}{dt} = h(x, u), \tag{2}$$

where $u(t)$ and $y(t)$ are the input and output of the memristor, respectively, x is the state variable, and $h(.)$ and $G(.)$ are functions related to a specific memristor. A simple generic memristor is presented as described by

$$i = G_0 x v, \tag{3a}$$

$$\frac{dx}{dt} = 2\tanh(x) - x + v = h(x, v), \tag{3b}$$

where $v(i)$ is the input voltage (output current), G_0x is the memductance function with intensity G_0, and $h(x,v)$ is the state expression of x. The circuit emulator is designed to validate its effectiveness and analyze its nonlinear characteristics to certify that the memristor is nonvolatile and locally active.

A. Circuit emulator of the memristor

The circuit emulator is shown in Fig. 1(a), which only contains a function unit $-\tanh(x)$, integrator U_0, analog multiplier A_0, and some resistances. The circuit schematic of $-\tanh(x)$ is depicted in Fig. 1(b), where there are a pair of differential transistors T_1 and T_2, two operational amplifiers U_1 and U_2, a current source I_0 at 1.1 mA, and some resistances at $R = 10\,\text{k}\Omega$, $R_F = 520\,\Omega$, and $R_\text{m} = 1\,\text{k}\Omega$. The circuit emulator consists of a small number of commercially available components, which shows a simple structure and exhibits low cost with easy physical implementation characteristics.

Values of $C_0 = 10\,\text{nf}$ and $\tau_0 = 1000$ ($\tau = \tau_0 t$) are chosen, and the circuit parameters are determined as $A_0 = 1$, $R_a = 100\,\text{k}\Omega$, $R_b = 100\,\text{k}\Omega$, $R_c = 50\,\text{k}\Omega$, and $R_0 = 1\,\Omega$. Circuit theory indicates that

$$i = A_0 x v, \tag{4a}$$

$$\frac{dx}{d\tau} = \frac{1}{R_c C_0}\tanh(x) - \frac{1}{R_b C_0}x + \frac{1}{R_a C_0}v, \tag{4b}$$

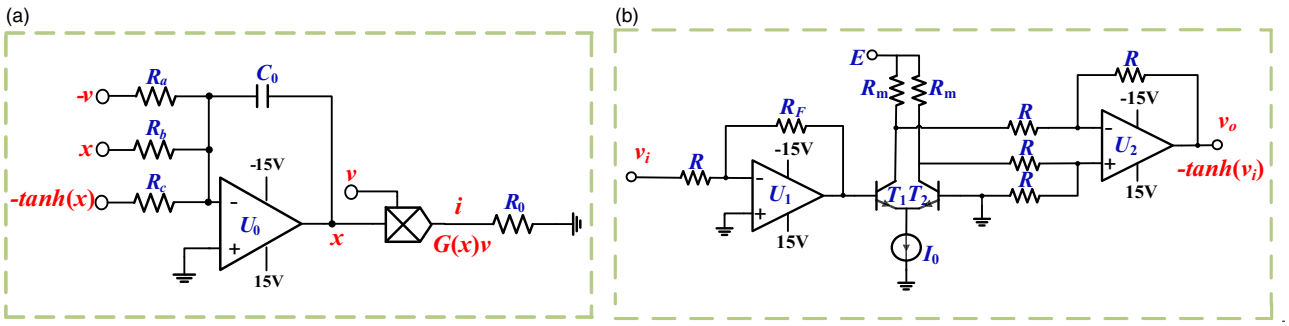

FIG. 1. (a) Circuit emulator topology and (b) –tanh(.) function circuit schematic.

where i and v are the current and voltage through the locally active memristor, respectively, and x is the state variable of the memristor. The circuit emulator corresponds to the simulation model for the locally active memristor defined by Eqs. (3a) and (3b).

B. Breadboard results

The frequency-dependent pinched hysteresis loop characteristics of the circuit emulator are explored through breadboard experiments. The experiments use a sinusoidal voltage source of $v = A\sin(2\pi f)$ with a fixed amplitude of $A = 2$ V using a signal generator. The pinched hysteresis loops with different frequencies are shown in Figs. 2(a1)–2(a3). Numerical simulations were performed to verify the effectiveness of the circuit emulator, as shown in Figs. 2(b1)–2(b3). Based on study in Ref. 30, the frequency f is given by $f = F\tau_0$. It is seen that both the breadboard experiments and the numerical simulations verify the fingerprints of the memristor.[36,37]

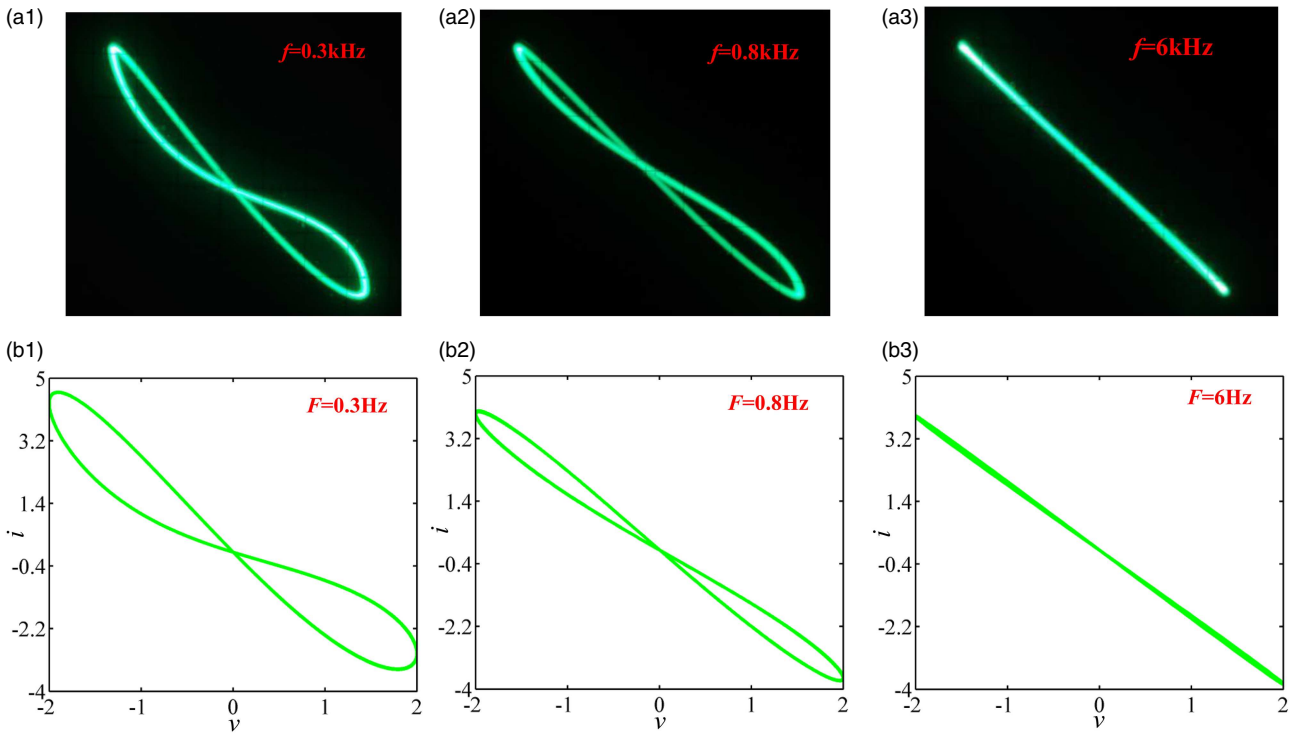

FIG. 2. Frequency-dependent pinched hysteresis loops. The top row is the results of the breadboard experiments and the bottom row is for the numerical simulations at frequencies of (1) 0.3 kHz, (2) 0.8 kHz, and (3) 6 kHz.

C. Verification of nonvolatile and locally active characteristics

The nonvolatile memristor retains its most recent memristance (memductance) state when powered off. The nonvolatile memristor theorem proposed by Chua suggests that a memristor with a scalar state variable x is nonvolatile if its POP intersects the x axis at two or more points with a negative slope.[17–20] The POP reveals changes in the state variable x of a memristor when the signal source is turned off. Hence, the POP of the memristor can be calculated by setting the voltage signal to $v = 0$ on the right-hand-side of Eq. (3b), as shown in Fig. 3(a). There are two intersections with the x axis that have negative slopes, indicating that the designed memristor is nonvolatile. Moreover, the POP reveals the equilibrium point (intersection with x axis) characteristics of the memristor, suggesting that those with negative (positive) slopes are stable (unstable). Thus, the equilibrium points Q_0 and Q_2 are asymptotically stable, but Q_1 is unstable. The moving direction of the memristor is marked by the arrowheads in Fig. 3(a), which point toward (away from) the stable (unstable) equilibrium points.

Exploring the DC voltage–current characteristics is an effective way to judge whether a memristor is locally active, which occurs when it has a negative slope curve in the DC V-I plot.[17] The DC V-I Loci can be derived from the parametric method.[38] Setting $(dx/dt) = 0$ in Eq. (3b) and partitioning the state variable x between -3 and 3 allows expressing the current and voltage in the following parametric form:

$$\begin{cases} V = -2\tanh(X) + X \\ I = G_0(-2X\tanh(X) + X^2) \end{cases}. \tag{5}$$

The DC V-I Loci are depicted in Fig. 3(b) when G_0 is equal to 1 ($G_0 > 0$). The slopes of the green curve and part of the red curve are negative; hence, the designed memristor is locally active. In Fig. 3(c), the DC V-I Loci with $G_0 = -1$ ($G_0 < 0$) are drawn as the black ($0 < x < 3$) and pink ($-3 < x < 0$) curves. Therefore, the locally active range is $x > 0$, which is a relatively wide region. Figures 3(b) and 3(c) indicate that the locally active range is also related to polarity of G_0.

D. Simulation characteristics

A memristor device with two different stable pinched hysteresis loops is called a bi-stable memristor. The stable pinched hysteresis loop pair is dependent on the initial value, amplitude, and frequency of the periodic signal v. When the amplitude ($A = 2$) and the frequency ($f = 1$ Hz) are fixed, the critical initial value $x^*(0)$ is approximately equal to -0.3119. The initial values of $x(0) = -0.31$ and $x(0) = -0.32$ are located on both sides of the critical value $x^*(0)$, and two completely different stable pinched hysteresis loops are drawn for $x(0) = -0.31$ (green curve) and $x(0) = -0.32$ (blue curve) in Fig. 4(a1). However, Fig. 4(b1) shows two identical hysteresis loops with different initial values of $x(0) = -0.1$ and $x(0) = 0.1$, both of which are larger than the critical initial value $x^*(0)$. On the other hand, the critical amplitude A^* is approximately 11.7769 V. Figure 4(a2) shows two stable pinched hysteresis loops with amplitudes of $A = 2$ V ($A < A^*$). Nevertheless, these join together absolutely at $A = 15$ V in Fig. 4(b2) ($A > A^*$). Here, the amplitude and special frequency are maintained at $A = 2$ V and $f^* = 0.1589$ Hz, respectively. Two stable pinched hysteresis loops are depicted in Fig. 4(a3) with $f = 0.6$ Hz ($f > f^*$), but they overlap at $f = 0.1$ Hz in Fig. 4(b3) ($f < f^*$).

The proposed locally active memristor is compared with reported locally active memristors from the basis of physical achievability, locally active features, etc., as given in Table I.

As is well-known, the use of multipliers in circuit implementations will increase its cost and reduce its stability. In general, the proposed locally active memristor has a simple structure with low cost, easy physical implementation, and wide locally active region characteristics.

III. LOCALLY ACTIVE MEMRISTOR NEURAL MODEL AND ITS EQUILIBRIUM POINTS

A. Neural model

The two-dimensional (2D) HR neuron model was simplified from the classical Hodgkin–Huxley model[39] by Hindmarsh and Rose.[40] It is believed that the HR neuron is effective and available to mimic electrical activity in the brain.[30,41] The autapse is a

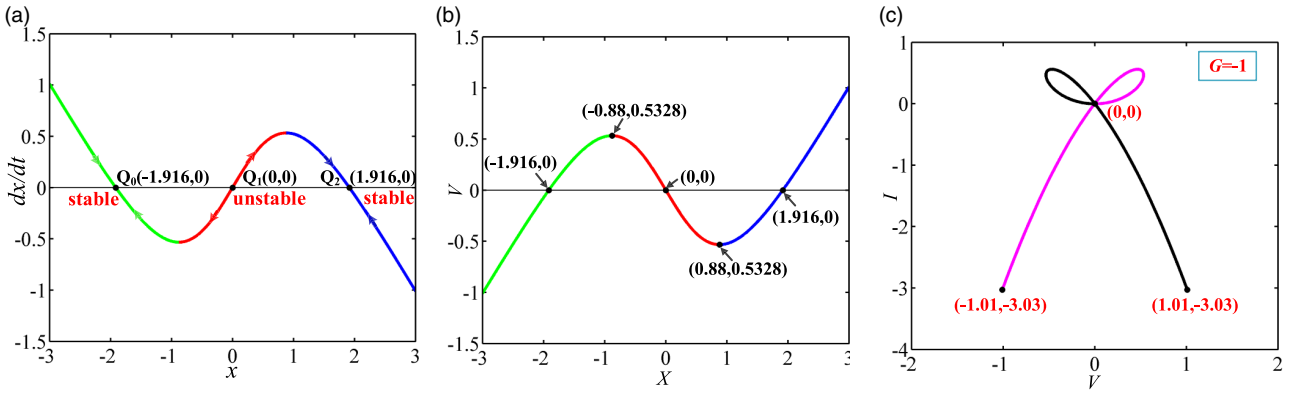

FIG. 3. (a) POP of the memristor, (b) DC V-I Loci of the memristor, and (c) locally active range for the state variable x.

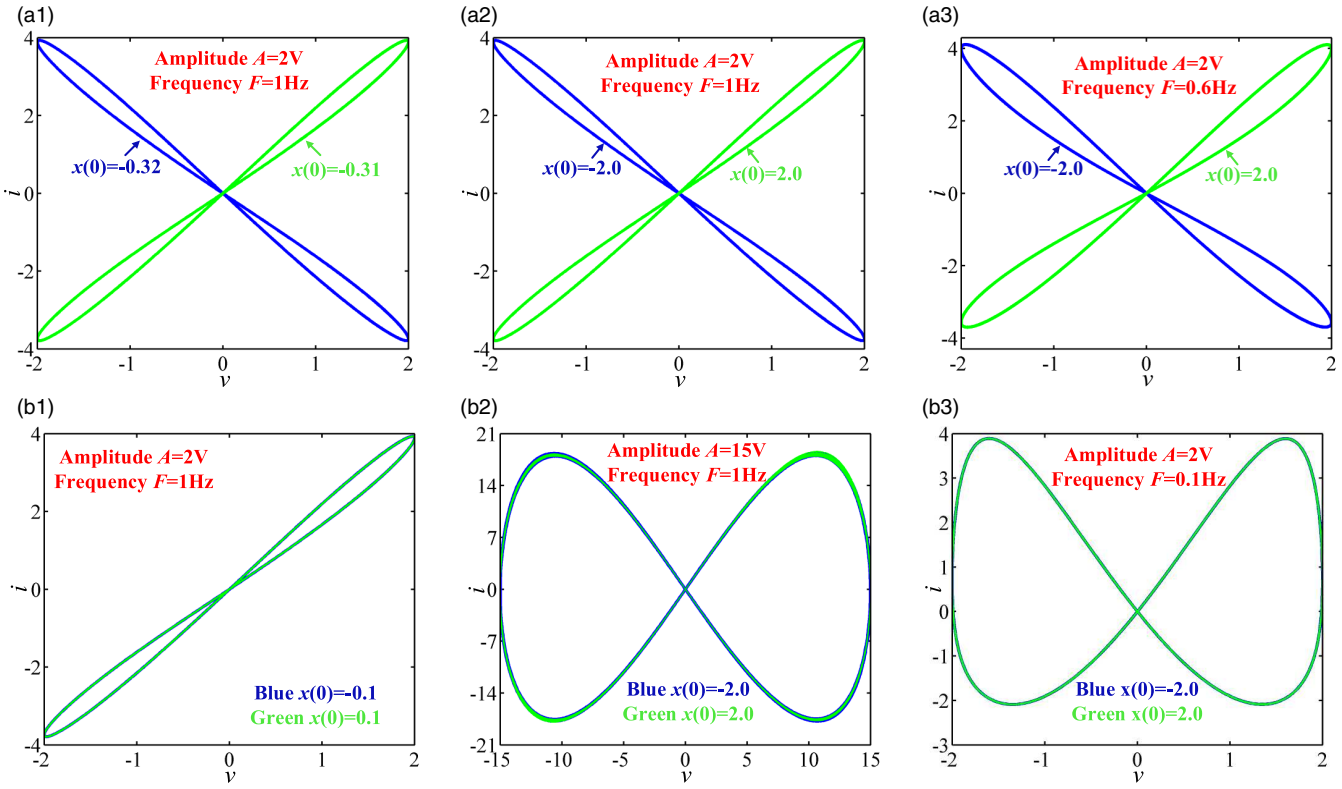

FIG. 4. Stable pinched hysteresis loops with different initial values, amplitudes, and frequencies: (a1) $x(0) = -0.32$ (blue curve) and $x(0) = -0.31$ (green curve); (b1) $x(0) = -0.1$ (blue curve) and $x(0) = -0.1$ (green curve); (a2) $A = 2$ V and (b2) $A = 15$ V; and (a3) $f = 0.8$ Hz and (b3) $f = 0.1$ Hz.

connection between a neuron and itself through a closed loop to regulate the membrane potential, which plays a significant role in numerous physiological activities of the brain. Therefore, a neural model composed of two 2D HR neurons using the proposed locally active memristor as an autapse is constructed. Meanwhile, the active processes of biological neurons are simulated using the activation function tanh(.). The connection structure is shown in Fig. 5.

Both x_1 and x_2 are the membrane potentials corresponding to the first (HR_1) and second (HR_2) neurons, respectively, y_1 and y_2 are the associated spiking variables, and a, b, c, and d are the 2D HR neuron model parameters, which are set as the classical values of $a = 1$, $b = 3$, $c = 1$, and $d = 5$. The mathematical expression for the model can be described as

$$\begin{cases} \frac{dx_1}{dt} = y_1 + 3{x_1}^2 - {x_1}^3 + k_1 W(x)\tanh(x_1) + k_2\tanh(x_2) \\ \frac{dx_2}{dt} = 1 - 5{x_1}^2 - y_1 \\ \frac{dx_2}{dt} = y_2 + 3{x_2}^2 - {x_2}^3 + k_3\tanh(x_1) + k_4\tanh(x_2) \\ \frac{dy_2}{dt} = 1 - 5{x_2}^2 - y_2 \\ \frac{dx}{dt} = 2\tanh(x) - x + x_1 \end{cases}, \quad (6)$$

TABLE I. Comparison of reported locally active memristors.

Items	Ref. 17	Ref. 19	Ref. 20	Proposed memristor
Memductance function	Quadratic term	Quadratic term	Quadratic and linear terms	Linear term
State equation	Piecewise linear	Cubic term and absolute value	Cubic and multiple quadratic terms	Linear term and tangent function
Physical realization	No	No	No	Yes
Locally active range	$0 < x < 10$	$2.5 < x < 3.75$	$x > 0$	$x > 0$ ($x < 0$)
Multiplication times	2	3	5	1
Memductance value	0+ or (0−)	0+ or (0−)	0+−	0+−

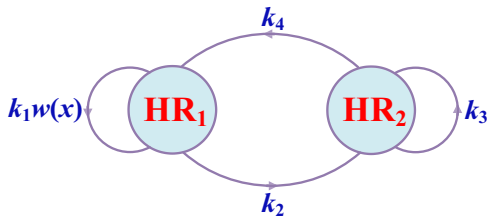

FIG. 5. Proposed neural model using the memristor.

where $k_1 W(x) = k_1 x$ represents the autapse described by the locally active memristor; x is the state variable; k_2, k_3, and k_4 are the connection parameters; and the activation function tanh(.) simulates the activation process of biological neurons.

B. Equilibrium point analysis

The analysis of equilibrium points reflects the local characteristics of a system. Setting the left-hand-side of Eq. (6) to 0 provides the equilibrium points as

$$E(x_1, 1 - 5{x_1}^2, x_2, 1 - 5{x_2}^2, x), \tag{7}$$

$$x_1 = x - 2\tanh(x), \tag{8}$$

where the values of x and x_2 can be solved using graphic analytic methods. The following functions are obtained by substituting Eqs. (7) and (8) into Eq. (6),

$$F_1(x, x_2) = 1 - 2[x - 2\tanh(x)]^2 - [x - 2\tanh(x)]^3 + k_1 x\tanh[x - 2\tanh(x)] + k_2\tanh(x_2) = 0, \tag{9}$$

$$F_2(x, x_2) = 1 - 2{x_2}^2 - {x_2}^3 + k_3\tanh[x - 2\tanh(x)] + k_4\tanh(x_2) = 0. \tag{10}$$

Equations (9) and (10) are drawn numerically in Figs. 6(a) and 6(b) for $k_1 = -0.2$ and $k_1 = -0.1$, respectively, when $k_2 = 1.2$, $k_3 = -0.9$, and $k_4 = -1$ are fixed.

The solutions for x and x_2 are the intersections of two functions in Figs. 6(a) and 6(b), which are determined using Newton's iterative method. When k_1 is equal to -0.2, the equilibrium points are $P_0(-1.5760, -11.4190, 0.6790, -1.3055, -3.5729)$, $P_1(-1.2154, -6.3865, 0.6638, -1.2029, -3.2089)$, and $P_2(0.6332, -1.0047. 0.2989, 0.5532, 2.6118)$. With $k_1 = -0.1$, the equilibrium point is $P_0(0.6666, -1.2215, 0.2904, 0.5785, 2.6466)$, giving three and one equilibrium points for $k_1 = -0.2$ and $k_1 = -0.1$, respectively. Therefore, the number of equilibrium points changes for different k_1.

IV. COMPLEX ELECTRICAL ACTIVITIES OF THE NEURAL MODEL

Bifurcation analysis, phase diagrams, and Lyapunov exponents are used to explore the electrical activity of the neural model. Bao's algorithm[30] and the MATLAB ODE23 algorithm are used in the bifurcation analysis and phase diagram, respectively, and there are 1000 iterations used in the Lyapunov exponent approach.

A. Oscillation only in locally active region

Based on Sec. II C, when the intensity k_1 of the locally active memristor is in the range of -0.2 to -0.08 ($k_1 < 0$), the locally active range of the memristor is $x(0) > 0$. The bifurcation diagram for k_1 was obtained by setting two initial values with the system parameters of $k_2 = 1.2$, $k_3 = -0.9$, and $k_4 = -1$ in which only $x(0)$ differs, as shown in Fig. 7(a). The blue curve corresponds to the initial value $(-1\ 0\ 1\ 0\ 2)$, in which the neural model exhibits complex and chaotic firing behaviors. In contrast, the red plot is related to the initial value $(-1\ 0\ 1\ 0\ -2)$, in which the neural model exhibits a quiescent firing behavior.

The bifurcation diagram with respect to $x(0)$ is plotted in Fig. 7(b) with the fixed system parameters of $k_1 = -0.15$, $k_2 = 1.2$, $k_3 = -0.9$, and $k_4 = -1$. The proposed neural model exhibits completely different firing behaviors with $x(0) = 0$ as the boundary, which is extremely complicated for all values of $x(0)$ in the locally active region and quiescent for all $x(0)$ in the locally passive region. Therefore, the simulation results suggest that oscillations only occur in the locally active region. Therefore, this study provides a way to explore complex electrical activities in neural systems.

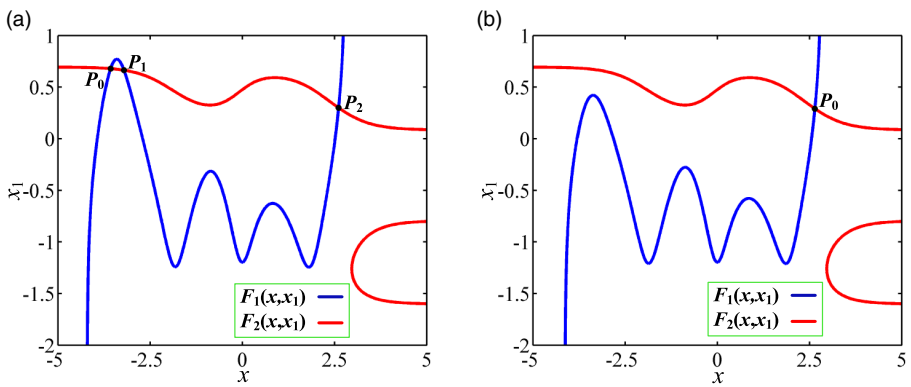

FIG. 6. Equilibrium points of the neural model for (a) $k_1 = -0.2$ and (b) $k_1 = -0.1$.

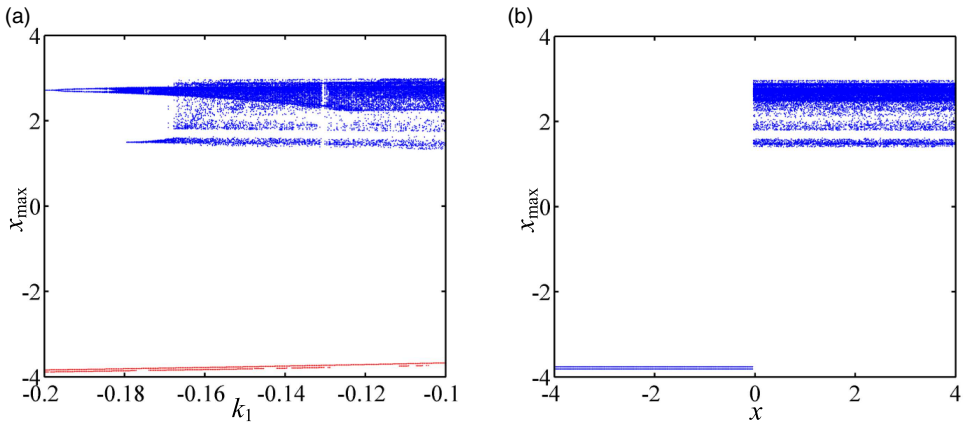

FIG. 7. (a) Bifurcation diagram for k_1 with initial values (−1 0 1 0 2) (blue curve) and (−1 0 1 0 −2) (red curve). (b) Bifurcation diagram for x with initial value (−1 0 1 0 x).

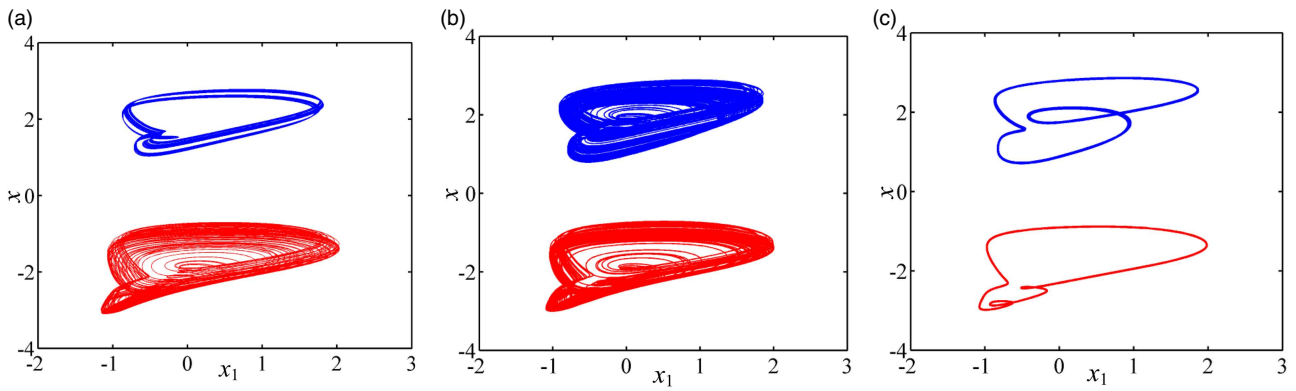

FIG. 8. Coexistence of different firing behaviors with different initial values of (−1 0 1 0 0) in blue and (0.4 −0.39 1 0 1) in red under k_1 values of (a) −0.147, (b) −0.1, and (c) −0.085.

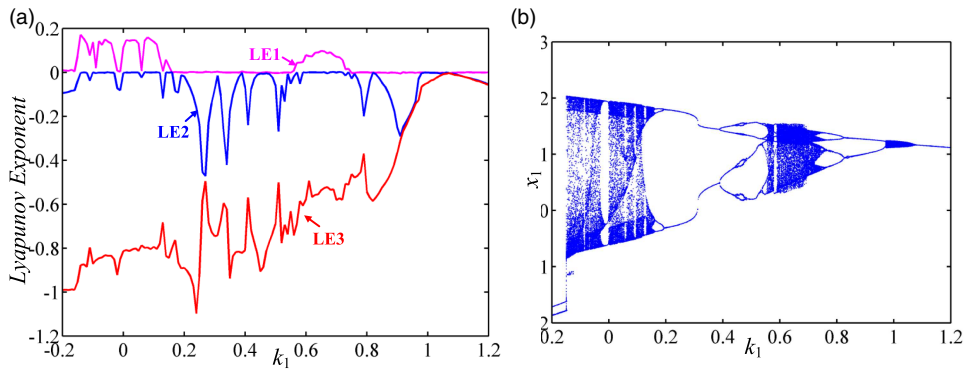

FIG. 9. Electrical behaviors of the proposed neural model with respect to k_1: (a) Lyapunov exponent graph and (b) bifurcation diagram of the membrane potential x_1.

B. Coexistence position symmetry of different attractors

The coexistence phenomenon is when different attractors appear under different initial conditions, which includes the attractor types and locations.[42–44] However, coexisting position symmetry for different attractors is a unique phenomenon. The phase diagrams for the x_1 and x planes are shown in Fig. 8. The system parameters are selected as $k_2 = 2$, $k_3 = -0.9$, and $k_4 = -1$ with several values of k_1 under different initial values. The quasi-period firing behavior and chaotic firing behavior appear in Fig. 8(a) for $k_1 = -0.147$. The coexistence of two different chaotic firing behaviors with different shapes emerges for $k_1 = -0.1$ is seen in Fig. 8(b), and the coexistence of the periodic-3 firing behavior with different shapes for $k_1 = -0.085$ appears in Fig. 8(c). Therefore, coexisting position symmetry firing behaviors are observed.

C. Lyapunov exponent and bifurcation analysis

The Lyapunov exponent approach is generally used to determine whether a system is in a chaotic state or not, while bifurcation analysis is an effective method to study nonlinear systems.[45] Therefore, Lyapunov exponent graphs and bifurcation diagrams for x_1 are drawn in Figs. 9(a) and 9(b), respectively, considering k_1 as the control parameter. The other system parameters are selected as $k_2 = 2$, $k_3 = -0.9$, and $k_4 = -1$ with the initial value (0.1 −0.1 −0.1 −0.1 −2). The Lyapunov exponent graph agrees with the bifurcation diagram. Moreover, the neural model shows abundant electrical behaviors for k_1 ranging from −0.2 to 1.2, such as quiescent, chaotic, and periodic firing behaviors for different cycles; forward and reverse period-doubling bifurcation behavior (remerging primary bubble); and tangent bifurcation and quasiperiodic firing behaviors. The membrane potential of HR_1 shows abundant electrical behavior as the intensity k_1 of the locally active memristor changes.

V. CIRCUIT IMPLEMENTATION

A. Schematics and equations of experimental circuit

The circuit is implemented to verify numeric simulations.[46] The operations of integration, addition, and subtraction of the system in Eq. (6) are accomplished by operational amplifiers connected with the capacitors and/or resistors, and the −tanh(.) circuit is given in Fig. 1(b). The main circuit scheme of the proposed system model implemented using a pure analog circuit is depicted in Fig. 10, which contains five circuit blocks for the physically implemented system. The circuit equation is described according to Kirchhoff's current law as

$$\begin{cases} \frac{dx_1}{d\tau} = \frac{1}{R_4C_1}y_1 + \frac{g_2}{R_1C_1}x_1^2 - \frac{g_1g_2}{R_5C_1}x_1^3 + \frac{g_7}{R_2C_1}x\tanh(x_1) \\ \qquad + \frac{1}{R_3C_1}\tanh(x_2) \\ \frac{dy_1}{d\tau} = \frac{v_1}{R_6C_2} - \frac{g_3}{R_7C_2}x_1^2 - \frac{1}{R_8C_2}y_1 \\ \frac{dx_2}{d\tau} = \frac{1}{R_{12}C_3}y_2 + \frac{g_5}{R_9C_3}x_2^2 - \frac{g_4g_5}{R_{13}C_3}x_2^3 - \frac{1}{R_{10}C_3}\tanh(x_1) \\ \qquad - \frac{1}{R_{11}C_3}\tanh(x_2) \\ \frac{dy_2}{d\tau} = \frac{v_2}{R_{14}C_4} - \frac{g_6}{R_{15}C_4}x_2^2 - \frac{1}{R_{16}C_4}y_2 \\ \frac{dx}{d\tau} = \frac{1}{R_cC_5}\tanh(x) - \frac{1}{R_bC_5}x + \frac{1}{R_aC_5}x_1 \end{cases} \quad . \qquad (11)$$

The state variables x_1, y_1, x_2, y_2, and x are voltages across the capacitors C_1, C_2, C_3, C_4, and C_5, respectively. It is assumed that the time constant is $\tau_0 = 1000$ ($\tau = \tau_0 t$) with a capacitance for the integrator of 10 nF. Based on the parameters of the system in Eq. (8), the value of other components is obtained as follows: $R_4 = 100\,\text{k}\Omega$, $R_1 = 3.33\,\text{k}\Omega$, $R_5 = 1\,\text{k}\Omega$, $R_2 = 10/k_1\,\text{k}\Omega$, $R_3 = 50\,\text{k}\Omega$, $R_6 = 100\,\text{k}\Omega$, $R_7 = 2\,\text{k}\Omega$, $R_8 = 100\,\text{k}\Omega$, $R_{12} = 100\,\text{k}\Omega$, $R_9 = 100\,\text{k}\Omega$, $R_{13} = 1\,\text{k}\Omega$, $R_{10} = 111.1\,\text{k}\Omega$, $R_{11} = 100\,\text{k}\Omega$, $R_{14} = 100\,\text{k}\Omega$, $R_{15} = 2\,\text{k}\Omega$, $R_{16} = 100\,\text{k}\Omega$, $R_{19} = 50\,\text{k}\Omega$, $R_{18} = 100\,\text{k}\Omega$, and $R_{17} = 100\,\text{k}\Omega$. It is noted that the resistor R_2 is an adjusting resistance and corresponds to the intensity of the locally active memristor.

B. Firing behavior verification

The physical circuit construction is executed on a breadboard. The multiplier AD633JN and operational amplifier TL082CD are supplied by a 15-V DC power supply along with a transistor S8050, a ceramic capacitor, and resistors. Two external bias voltages V_1 and V_2 are supplied from a DC voltage source. The output results are captured using a digital oscilloscope. The induced initial voltages for the five capacitors are randomly obtained by repeatedly cycling the power supply. The firing patterns are observed by adjusting R_2 as

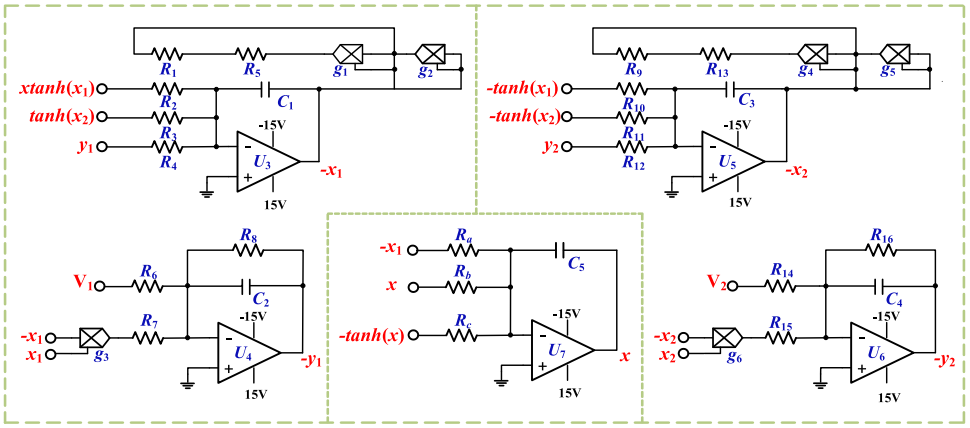

FIG. 10. Main circuit of the proposed neuron model.

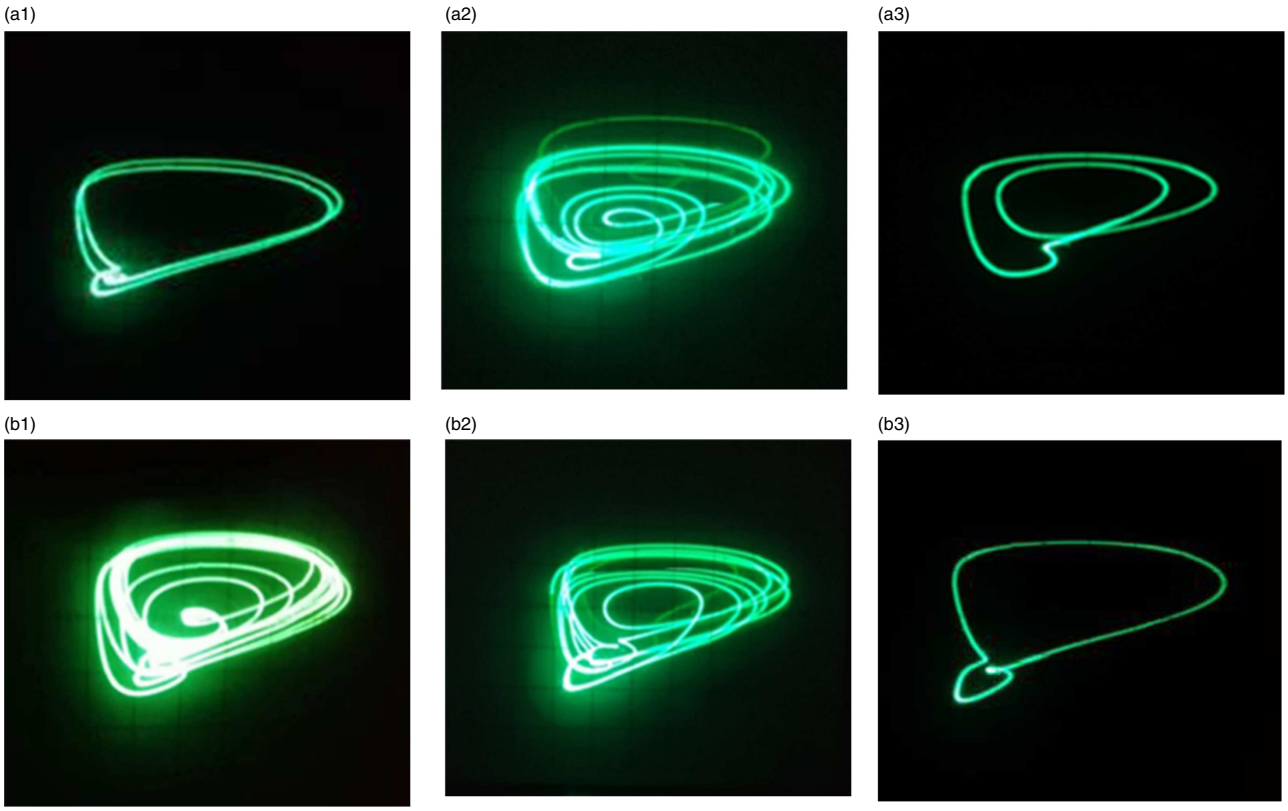

FIG. 11. Experimental measurement results for the (a1) quasi-period with $R_2 = 65\,k\Omega$, (b1) chaotic firing with $R_2 = 65\,k\Omega$, (a2) chaotic firing with $R_2 = 100\,k\Omega$, (b2) chaotic firing with $R_2 = 100\,k\Omega$, (a3) three-period firing with $R_2 = 120\,k\Omega$, and (b3) three-periodic firing with $R_2 = 120\,k\Omega$.

shown in Fig. 11. There is a slight dissimilarity between the theoretical and actual R_2 values of 65 kΩ and 120 kΩ, respectively, as caused by system errors and parasitic parameters.

VI. CONCLUSION

This article proposes a locally active memristor and explores its application in HR neurons. The circuit emulator is presented using common electronic components, and the nonvolatile and locally active characteristics of the memristor are verified using the POP and DC *V-I* plot, respectively. Both the breadboard experiments and simulation results verify the effectiveness of the locally active memristor. Compared with reported locally active memristors, the advantages of the presented memristor are its simple structure and excellent characteristics, such as low cost, easy physical implementation, and a wide locally active region. Moreover, the locally active memristor is used as an autapse to construct a neural model and explore its application as HR neurons. The electrical activities are investigated using bifurcation diagrams, phase portraits, and Lyapunov exponent graphs, with associated hardware experiments. A new neurodynamic behavior of coexisting position symmetry for different attractors is discovered for the proposed neural model. It is believed that this study contributes to the theoretical research of memristors and the exploration of unique electrical activities in the brain. In future work, it may be possible and valuable to design a locally active memristor with better characteristics and explore other new neurodynamic behaviors in the neural model based on locally active memristors.

ACKNOWLEDGMENTS

This work was supported by the National Natural Science Foundation of China (NNSFC; Nos. 91964108 and 61971185).

REFERENCES

[1] L. Chua, "Memristor-the missing circuit element," IEEE Trans. Circuit Theory **18**(5), 507–519 (1971).
[2] D. B. Strukov *et al.*, "The missing memristor found," Nature **453**(7191), 80 (2008).
[3] C. Wang *et al.*, "Synchronization stability and pattern selection in a memristive neuronal network," Chaos **27**(11), 113108 (2017).
[4] K. Rajagopal *et al.*, "Spiral waves in externally excited neuronal network: Solvable model with a monotonically differentiable magnetic flux," Chaos **29**(4), 043109 (2019).
[5] W. Yao *et al.*, "Hybrid multisynchronization of coupled multistable memristive neural networks with time delays," Neurocomputing **363**, 281–294 (2019).

[6]C. Wang *et al.*, "Memristor-based neural networks with weight simultaneous perturbation training," Nonlinear Dyn. **95**(4), 2893–2906 (2019).
[7]D. B. Strukov, "Endurance-write-speed tradeoffs in nonvolatile memories," Appl. Phys. A **122**(4), 302 (2016).
[8]S. Kvatinsky *et al.*, "VTEAM: A general model for voltage-controlled memristors," IEEE Trans. Circuits Syst. II Exp. Briefs **62**(8), 786–790 (2015).
[9]J. Ruan *et al.*, "Fractional-order simplest memristor-based chaotic circuit with new derivative," European Phys. J. Plus **133**(1), 3 (2018).
[10]L. Zhou, W. Chunhua, and Z. Lili, "A novel no-equilibrium hyperchaotic multi-wing system via introducing memristor," Int. J. Circ. Theor. Appl. **46**(1), 84–98 (2018).
[11]C. Wang, L. Xiaoming, and X. Hu, "Multi-piecewise quadratic nonlinearity memristor and its 2 N-scroll and 2 N+ 1-scroll chaotic attractors system," Chaos **27**(3), 033114 (2017).
[12]F. Yu *et al.*, "Secure communication scheme based on a new 5D multistable four-wing memristive hyperchaotic system with disturbance inputs," Complexity **2020**, 5859273.
[13]L. Chua, "If it's pinched it's a memristor," Semicond. Sci. Technol. **29**(10), 104001 (2014).
[14]L. O. Chua, "Local activity is the origin of complexity," Int. J. Bifurcation Chaos **15**(11), 3435–3456 (2005).
[15]B. Muthuswamy and L. O. Chua, "Simplest chaotic circuit," Int. J. Bifurcation Chaos **20**(5), 1567–1580 (2010).
[16]S. Kumar, S. S. J. Paul, and W. R. Stanley, "Chaotic dynamics in nanoscale NbO2 mott memristors for analogue computing," Nature **548**(7667), 318 (2017).
[17]C. H. U. A. Leon, "Everything you wish to know about memristors but are afraid to ask," Radioengineering **24**(2), 319 (2015).
[18]I. Z. Mannan, C. Hyuncheol, and K. Hyongsuk, "Chua corsage memristor oscillator via hopf bifurcation," Int. J. Bifurcation Chaos **26**(04), 1630009 (2016).
[19]H. Chang *et al.*, "Dynamic analysis of a bistable bi-local active memristor and its associated oscillator system," Int. J. Bifurcation Chaos **28**(08), 1850105 (2018).
[20]P. Jin *et al.*, "A locally active memristor and Its application in a chaotic circuit," IEEE Trans. Circuits Syst. II Exp. Briefs **65**(2), 246–250 (2017).
[21]H. Kim *et al.*, "Neural synaptic weighting with a pulse-based memristor circuit," IEEE Trans. Circuits Syst. I Reg. Papers **59**(1), 148–158 (2011).
[22]Z. I. Mannan, S. P. Adhikari, C. Yang, R. K. Budhathoki, H. Kim, and L. Chua, "Memristive imitation of synaptic transmission and plasticity," IEEE Trans. Neural Netw. Learn. Syst. **30**(11), 3458–3470 (2019).
[23]Y. Xu, H. Ying, Y. Jia, J. Ma, and T. Hayat, "Autaptic regulation of electrical activities in neuron under electro-magnetic induction," Sci. Rep. **7**, 43452 (2017).
[24]X. Song, H. Wang, and Y. Chen, "Autapse-induced firing patterns transitions in the Morris-Lecar neuron model," Nonlinear Dyn. **96**(4), 2341–2350 (2019).
[25]G. Ren, X. Ying, and W. Chunni, "Synchronization behavior of coupled neuron circuits composed of memristors," Nonlinear Dyn. **88**(2), 893–901 (2017).
[26]Y. Xu *et al.*, "Synchronization between neurons coupled by memristor," Chaos Soliton. Fract. **104**, 435–442 (2017).
[27]F. Xu *et al.*, "Synchronous dynamics in neural system coupled with memristive synapse," Nonlinear Dyn. **92**(3), 1395–1402 (2018).
[28]M. Lv and M. Jun, "Multiple modes of electrical activities in a new neuron model under electromagnetic radiation," Neurocomputing **205**, 375–381 (2016).
[29]K. S. Thottil and P. I. Rose, "Influence of memristor and noise on h–r neurons," Nonlinear Dyn. **95**(1), 239–257 (2019).
[30]H. Bao *et al.*, "Hidden bursting firings and bifurcation mechanisms in memristive neuron model with threshold electromagnetic induction," IEEE Trans. Neural Netw. Learn. Syst. **31**, 502–511 (2019).
[31]Q. Xu *et al.*, "Two-neuron-based non-autonomous memristive Hopfield neural network: Numerical analyses and hardware experiments," AEU-Int. J. Electron. Commun. **96**, 66–74 (2018).
[32]B. Bao *et al.*, "Coexisting behaviors of asymmetric attractors in hyperbolic-type memristor based Hopfield neural network," Front. Comput. Neurosci. **11**, 81 (2017).
[33]L. Chua, S. Valery, and K. Hyongsuk, "Neurons are poised near the edge of chaos," Int. J. Bifurcation Chaos **22**(04), 1250098 (2012).
[34]P. M. Sah, K. Hyongsuk, and C. O. Leon, "Brains are made of memristors," IEEE Circ. Syst. Mag. **14**(1), 12–36 (2014).
[35]L. O. Chua, "Memristor, Hodgkin Huxley, and edge of chaos," Nanotechnology **24**(38), 383001 (2013).
[36]S. P. Adhikari *et al.*, "Three fingerprints of memristor," IEEE Trans. Circuits Syst. I Reg. Papers **60**(11), 3008–3021 (2013).
[37]Q. Zhao, C. Wang, and X. Zhang, "A universal emulator for memristor, memcapacitor, and meminductor and its chaotic circuit," Chaos **29**(1), 013141 (2019).
[38]L. O. Chua and A. R. Rohrer, *Nonlinear Network Analysis: The Parametric Approach* (Illinois Univ Urbans Coordinated Science Lab, 1964), Vol. 224.
[39]L. A. Hodgkin and A. F. Huxley, "A quantitative description of membrane current and its application to conduction and excitation in nerve," J. Physiol. **117**(4), 500–544 (1952).
[40]J. L. Hindmarsh and R. M. Rose, "A model of the nerve impulse using two first-order differential equations," Nature **296**(5853), 162 (1982).
[41]H. Bao, L. Wenbo, and H. Aihuang, "Coexisting multiple firing patterns in two adjacent neurons coupled by memristive electromagnetic induction," Nonlinear Dyn. **95**(1), 43–56 (2019).
[42]L. Zhou *et al.*, "Various attractors, coexisting attractors and antimonotonicity in a simple fourth-order memristive twin-T oscillator," Int. J. Bifurcation Chaos **28**(04), 1850050 (2018).
[43]G. Wang *et al.*, "Coexisting multiple attractors and riddled basins of a memristive system," Chaos **28**(1), 013125 (2018).
[44]F. Yu *et al.*, "Chaos-based application of a novel multistable 5D memristive hyperchaotic system with coexisting multiple attractors," Complexity **2020**, 8034196.
[45]H. Lin and W. Chunhua, "Influences of electromagnetic radiation distribution on chaotic dynamics of a neural network," Appl. Math. Comput. **369**, 124840 (2020).
[46]F. Yu *et al.*, "Analysis and FPGA realization of a novel 5D hyperchaotic four-wing memristive system, active control synchronization, and secure communication application," Complexity **2019**, 1–18.